2015

Aerosol Optical Properties Over Mount Song, a Rural Site in Central China

Lunche Wang
China University of Geosciences Wuhan

Wei Gong
Wuhan University

Ramesh P. Singh
Chapman University, rsingh@chapman.edu

Xiangao Xia
Chinese Academy of Sciences

Huizheng Che
Chinese Academy of Meteorological Sciences

See next page for additional authors

Recommended Citation

Wang, Lunche, et al. "Aerosol Optical Properties over Mount Song, a Rural Site in Central China." *Aerosol and Air Quality Research* 15.5 (2015): 2051-2064. doi: 10.4209/aaqr.2014.12.0335

Aerosol Optical Properties Over Mount Song, a Rural Site in Central China

Authors

Lunche Wang, Wei Gong, Ramesh P. Singh, Xiangao Xia, Huizheng Che, Ming Zhang, and Hong Lin

Aerosol and Air Quality Research, 15: 2051–2064, 2015

ISSN: 1680-8584 print / 2071-1409 online
doi: 10.4209/aaqr.2014.12.0335

Aerosol Optical Properties over Mount Song, a Rural Site in Central China

Lunche Wang[1,2*], Wei Gong[3,4], Ramesh P. Singh[5], Xiangao Xia[6,7], Huizheng Che[8], Ming Zhang[3], Hong Lin[9]

[1] *Department of Geography, School of Earth Sciences, China University of Geosciences, Wuhan 430074, China*
[2] *State Key Laboratory of Biogeology and Environmental Geology, China University of Geosciences, Wuhan 430074, China*
[3] *State Key Laboratory of Information Engineering in Surveying, Mapping and Remote Sensing, Wuhan University, Wuhan, Hubei province, 430079, China*
[4] *Collaborative Innovation Center for Geospatial Technology, Wuhan 430079, China*
[5] *School of Earth and Environmental Sciences, Schmid College of Science and Technology, Chapman University, Orange CA 92866, USA*
[6] *Laboratory for Middle Atmosphere and Global Environment Observation, Institute of Atmospheric Physics, Chinese Academy of Sciences, Beijing 100029, China*
[7] *Collaborative Innovation Center on Forecast and Evaluation of Meteorological Disasters, Nanjing University of Information Science & Technology, Nanjing, 210044, China*
[8] *Key Laboratory for Atmospheric Chemistry, Institute of Atmospheric Composition, Chinese Academy of Meteorological Sciences, CMA, Beijing 100081, China*
[9] *School of Physics and Electronic-Information Engineering, Hubei Engineering University, Xiaogan 432000, Hubei, China*

ABSTRACT

Seasonal variations of aerosol optical depth (AOD), Ångström exponent (α), single scattering albedo (SSA), water vapor content (WVC), aerosol size distribution and refractive index at Mount Song, a rural site in Central China are analyzed using ground-based sunphotometer data for the period April 2012 to May 2014 for the first time. The results show that the area is highly polluted even the major anthropogenic emission sources are far away. Seasonal mean AOD is high (0.72 ± 0.52) during summer (June–August) season and low (0.51 ± 0.38) during autumn (September–November) season. The monthly mean α is very low (0.81 ± 0.30) in the month of April and very high (1.32 ± 0.23) in the month of September with annual average value 1.1. Analysis of the frequency distributions of AOD and α in each season indicates presence of fine-mode particles. Strong seasonal variations in SSA is likely due to local biomass burning and regional transport of anthropogenic aerosol particles, Seasonal mean SSA at 440 nm wavelength are 0.89 ± 0.04, 0.91 ± 0.06, 0.89 ± 0.07 and 0.92 ± 0.05, respectively during spring, summer, autumn and winter seasons. It is also shown that the scattering capacity of the fine-mode particles is relatively higher during summer compared to other seasons. The aerosol volume size distributions show pronounced seasonal variations in volume concentration, peak radius and the fine-mode particles are evidently dominant during summer season due to the hygroscopic growth. A distinct seasonal variations in aerosol parameters confirm the transport of polluted air mass at Mount Song.

***Keywords*:** Aerosol optical properties; Ground-based measurements; Mount Song; Central China.

INTRODUCTION

Aerosols are solid or liquid particles in the atmosphere, their concentrations and type of particles influence the global and regional climates, directly through the interaction with solar radiation and indirectly modifying cloud microphysics (Albrecht, 1989). The aerosol optical and physical properties (aerosol optical depth-AOD, Ångström exponent, single scattering albedo (SSA), aerosol size distribution and refractive index) are important parameters controlling the aerosol radiative forcing at the surface and at the top of the atmosphere (Breon *et al.*, 2002; Cheng *et al.*, 2008). Due to the low spatial and temporal variations of aerosols, physical and chemical properties of aerosols still remain as one of the major uncertainties in estimating climatic forcing (IPCC, 2007; He *et al.*, 2012). In order to better understand aerosol optical properties and the effects on climate and atmospheric environment, long term systematic measurements of aerosol

* Corresponding author.
Tel.: 86-13349889828; Fax: 86-027-86087728
E-mail address: lunchewang@whu.edu.cn

parameters are needed.

Ground-based remote sensing is ideal for continuous observations of column-integrated aerosol properties in key locations around the world, which have used for validation of satellite derived products (Tripathi *et al.*, 2005; Prasad and Singh, 20005; Che *et al.*, 2008; Prasad and Singh, 2009; Guo *et al.*, 2010; Kumar *et al.*, 2013). Many ground-based observation networks have been established around the world, such as the Aerosol Robotic Network (AERONET) and the Global Atmosphere Watch (GAW) of World Meteorological Organization (WMO) (Holben *et al.*, 1998; Goloub *et al.*, 2007; Estellés *et al.*, 2012). In recent years, aerosols over East Asia, especially over China, have attracted considerable attention because of their high surface concentrations and the co-existence of dust, industrial pollutants and biomass burning aerosols (Li *et al.*, 2007; Xia *et al.*, 2007; Cao *et al.*, 2014; Zheng *et al.*, 2014). Numerous observational studies on the aerosol optical properties have been carried out in China (Xia *et al.*, 2006; Yu *et al.*, 2009a; Che *et al.*, 2013), efforts have also been made in establishing ground-based remote sensing networks in China, such as the Aerosol Remote Sensing Network (CARSNET) developed by the China Meteorological Administration (Che *et al.*, 2009) and the Chinese Sun Hazemeter Network developed by the Chinese Academy of Sciences (Wang *et al.*, 2011). Xia *et al.* (2006) first reported the seasonal variability of aerosol optical properties over Beijing; Ge *et al.* (2010) investigated the dust aerosol properties and radiative forcing over the northwestern China. Most of aerosol studies in China are mainly focused on Beijing-Tianjin-Hebei area (Xia *et al.*, 2007; Che *et al.*, 2014a), Yangtze Delta region (Pan *et al.*, 2010) and some heavy-polluted regions (Li *et al.*, 2007; Che *et al.*, 2014b; Zhuang *et al.*, 2014). Only few studies on aerosol properties using ground-based measurements have been carried out over rural sites in Central China (Wang *et al.*, 2015), which is important to understand the aerosol properties and dynamics of aerosol properties from rural to urban and urban to rural areas.

Henan Province is one of the most populated (more than 105 million people) areas in China, which is a national key production base for wheat and cotton crops in Central China (Lu *et al.*, 2013). Due to rapid population and economic growth, anthropogenic aerosols have dramatically increased in recent decades, that show effects on the local crop production, ecological environment and regional climate (Liu *et al.*, 2012). Aerosol optical properties in this area are highly complex and variable from those observed in the eastern China and other European countries (Che *et al.*, 2015; Wang *et al.*, 2015). For quantification, characterization and to understand the seasonal dynamics of aerosols and their impacts on radiation budget and regional climate ground-based observations at a closed network are important. In this study, we present results of aerosol parameters for two years periods (April 2012–May 2014) obtained from a ground sunphotometer deployed at a rural site (34°31′N, 113°07′E) in the Central China. Most of the aerosol parameters show strong seasonal variations and dynamics and transport of polluted air mass from surrounding areas.

SITE, INSTRUMENT AND METHODOLOGY

A Cimel sunphotometer CE-318 manufactured by the CIMEL Electronique Company, France was installed at the top of a building near the Songshan Artificial Target site (34°31′N, 113°07′E, 460 m above sea level) at Mount Song (Fig. 1), Dengfeng city in Henan Province, China in the month of April, 2012. Mount Song is the first target site in China for validation of satellite remote sensor on-orbit performance assessment (Li *et al.*, 2014). Dengfeng city (about 10 km from the observational site) is one of the most well known spiritual centres of China, home to various religious institutions and temples, such as the Taoist Zhongyue Temple, the Buddhist Shaolin Temple, as well as the Confucian Songyang Academy, hence its poetic expression derived from Chinese literature as the spiritual "centre of heaven and earth" (Lao and Wang, 1999, Liu *et al.*, 2012). This region experiences a typical north temperate monsoon climate, with an annual average temperature of 14.3°C and an annual average rainfall 640.9 mm, the monthly mean air temperature is lowest (0.2°C) in the month of January and highest (27.3°C) in the month of July (Li *et al.*, 2008).

The sunphotometer CE-318 makes direct spectral solar radiation measurements within a 1.2° full field-of-view every 15 min at 9 wavelengths 340, 380, 440, 500, 675, 870, 940, 1020 and 1640 nm, solar radiation at wavelength measured at 940 nm is used to obtain the total precipitable water content, and the other wavelengths are used for deriving the spectral AOD (total uncertainty is about 0.01–0.02) (Holben *et al.*, 1998; Eck *et al.*, 1999; Dubovik *et al.*, 2000; Che *et al.*, 2009). The sunphotometer is annually calibrated using CARSNET (China Meteorological Administration Aerosol Remote Sensing Network) reference instrument to ensure the accuracy and reliability of the data, the detailed calibration procedures are discussed in detail (Che *et al.*, 2009; Tao *et al.*, 2014b).

The AODs data are calculated using the ASTPwin software (Cimel Ltd. Co.) for Level 1.0 AODs (raw result without cloud-screening), Level 1.5 AODs (cloud-screened AOD following methodology discussed in detail by Smirnov *et al.* (2000) and the Ångström exponents are calculated at two wavelengths 440 and 870 nm as discussed by many (Che *et al.*, 2009, 2013; Zhao *et al.*, 2013; Tao *et al.*, 2014a). Aerosol optical properties are retrieved using almucantar measurements of Cimel sunphotometer according to Dubovik and King (2000) and Dubovik *et al.* (2002, 2006). The Cimel sky radiance measured at wavelengths 440, 675, 870, and 1020 nm, in conjunction with direct sun AODs at the same wavelengths, these parameters were used to retrieve aerosol size distributions (from 0.05 to 15 μm) and single scattering albedo (total, fine and coarse particles) (Eck *et al.*, 2010). All the measurements were checked manually to ensure good data quality, for example, some high AODs usually caused by the cloud, after checking the MODIS Level-1B granule (MOD02_1km) images, such AODs values were deleted. In order to ensure the data quality and represent the daily/monthly mean values, only data ≥ 10 times per day were selected for the daily average calculation, and daily observations > 10 in each month are regarded for

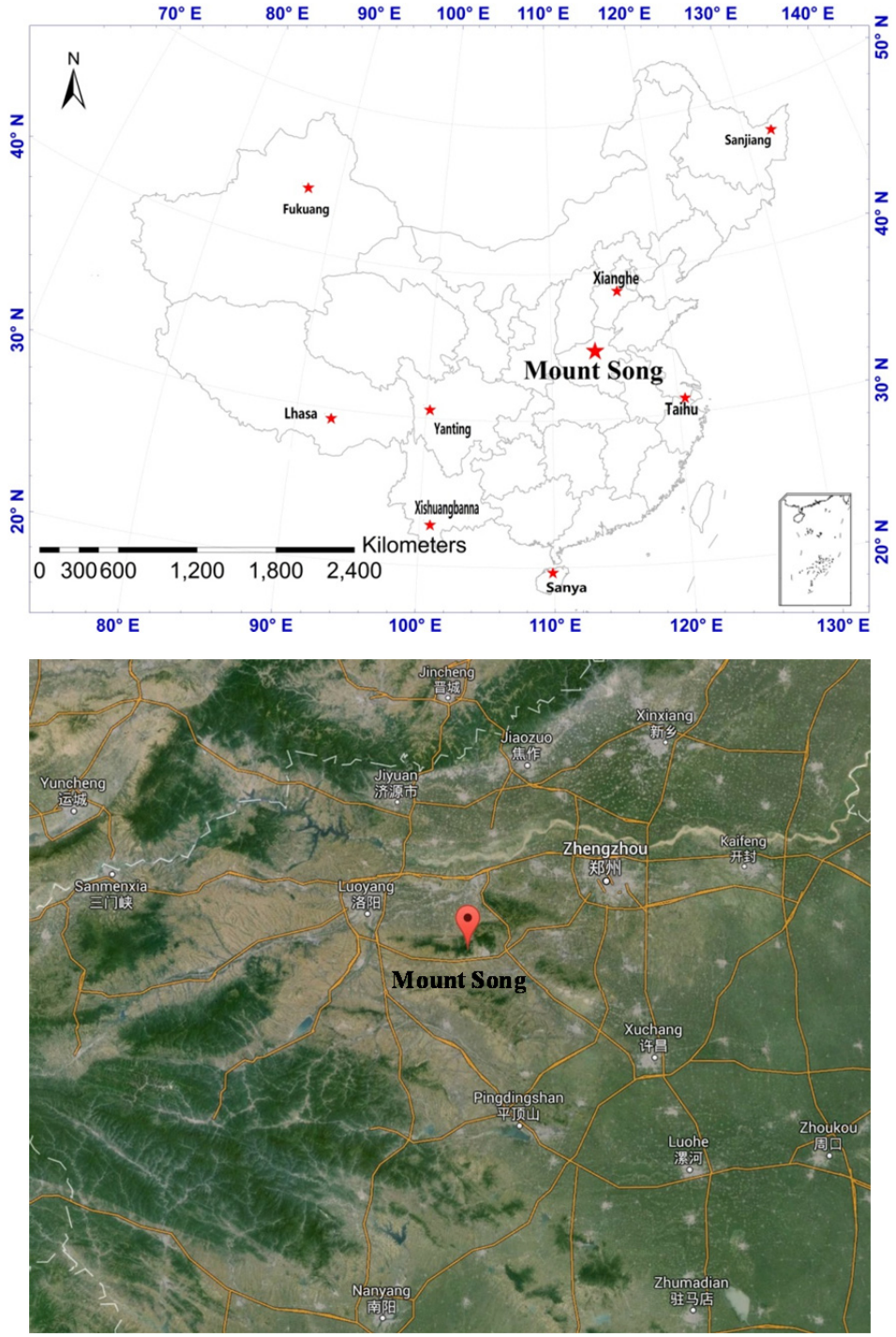

Fig. 1. The location of Mount Song and surrounding area in China.

monthly calculation. This data control procedure is widely adopted by the China Meteorological Administration Aerosol Remote Sensing Network (Che *et al.*, 2009; 2013; Zhao *et al.*, 2013; Tao *et al.*, 2014a). Finally, daily and monthly mean values of AODs, α and other aerosol parameters for the periods April, 2012 to May, 2014 are obtained from 353 daily observations, details of monthly measurements are given in Table 1.

The MODIS aerosol products have been comprehensively validated and analyzed over land on a global scale using observations from Aerosol Robotic Network (AERONET) (Remer *et al.*, 2005; Levy *et al.*, 2010). There are several algorithms producing aerosol products from MODIS, the 3 km aerosol product MOD043K from Aqua satellite for the period April 2012–May 2014 are considered for validation of the satellite data with ground based sunphotometer CE318 observations. The product is created using similar structure, inversion methods and lookup tables as in the basic 10 km Dark Target products, the detailed inversion algorithm about MOD043K is discussed in detail by Remer

Table 1. Statistics of the measurements at Mount Song.

Month	Jan	Feb	Mar	Apr	May	Jun	Jul	Aug	Sep	Oct	Nov	Dec
Days	28	17	33	35	32	25	25	27	29	37	40	25
Observations	638	287	626	717	634	389	356	413	532	812	1123	664

et al. (2013). In the present study, MODIS derived AOD_{550nm} data are compared with ground measured sunphotometer data following the method of Ichoku *et al.* (2002). The observed AOD_{550nm} at Mount Song are averaged within ± 30 min of the satellite's passing and the MODIS data are averaged over a 15 km area centred at the ground stations (including at least five pixels). Statistical correlation analyses for the two data sets are shown in Fig. 2. A good correlation (R^2 = 0.9) between ground and satellite (MODIS) derived AOD_{550nm}, 83% of the values are found within expected error (RMSE 0.11). Such high correlations provide confidence on our ground and satellite derived AODs to study the aerosol optical properties at the Mount Song.

RESULTS AND DISCUSSION

Aerosol Optical Depth, Ångström Exponent and Water Vapor

The annual mean AOD_{500nm} at Mount Song during the period 2012–2014 is about 0.60, which is lower than those observed at Beijing (0.841, annual mean AOD_{500nm} during 2002–2007) (Xia *et al.*, 2006; Yu *et al.*, 2009a). The annual mean AOD_{500nm} at Xianghe, Taihu and Yanting are 0.82 (Li *et al.*, 2007), 0.77 (Li *et al.*, 2007) and 0.79 (Wang *et al.*, 2011), which indicate that aerosol loading at Mount Song in Central China is lower compared to Beijing, Xianghe, Taihu and other sites in China. However, the average AOD_{500nm} at Mount Song is also higher compared to other locations: Xinglong, Lanzhou, Xishuangbanna, Lhasa, Sanya, Fukang and Sanjiang were mean AOD_{500nm} respectively varies as 0.28, 0.38, 0.45, 0.15, 0.23, 0.29 and 0.21 (Yu *et al.*, 2009b; Wang *et al.*, 2011; Zhu *et al.*, 2014).

Fig. 3 shows the monthly variations of AODs, α and water vapor content, the monthly mean AOD_{500nm} increases from 0.45 in the month of December to 1.15 in the month of February. The seasonal mean AOD_{500nm} is 0.6 ± 0.42, 0.72 ± 0.52, 0.51 ± 0.42 and 0.64 ± 0.58, respectively, for spring, summer, autumn and winter seasons. The high AODs during summer months (June–August) are likely to be associated with dust events (Cao *et al.*, 2014). High water vapor content in the atmosphere during summer months favor the hygroscopic growth of fine mode aerosols (Eck *et al.*, 2005, Gautam *et al.*, 2007). During autumn and winter seasons, this area is mainly controlled by Mongolian Anti-cyclone; the weather conditions favor the lower AODs occurrences (Yu *et al.*, 2009a; Pan *et al.*, 2010).

The monthly variations of α is opposite to the AOD, the value of α is low in the month of April (0.81 ± 0.30) and high in the month of September (1.32 ± 0.23) (Fig. 3(b)), mean monthly α value is greater than 0.80 showing presence of fine particles. The mean value of α is 0.93, 1.26, 1.16 and 1.23, respectively, for spring, summer, autumn and winter seasons at Mount Song. Generally, α larger than 0.80 can be regarded as fine or small particles, so Mt. Song mainly consists of fine particles. But during spring α is lower compared to other seasons, which is likely due to the variability in dust sources and mixing of dust with surrounding anthropogenic emissions. The strong seasonal variations of aerosol parameters could be related to the sources of aerosol, for example, relatively low values of α are the characteristics of coarse aerosol particles during spring season associated to dust events in the Northwest China.

High values of water vapor content (WVC) is generally observed during summer season (Fig. 3(c)), which is consistent with the climatic conditions (temperate monsoon) in the area. The minimum monthly average of WVC is about 0.35 cm in the month of January, which is gradually increases from the month of February to August, with a maximum value (3.62 cm) of WVC. A poor correlation between AOD and α with WVC (R^2 < 0.1) is observed,

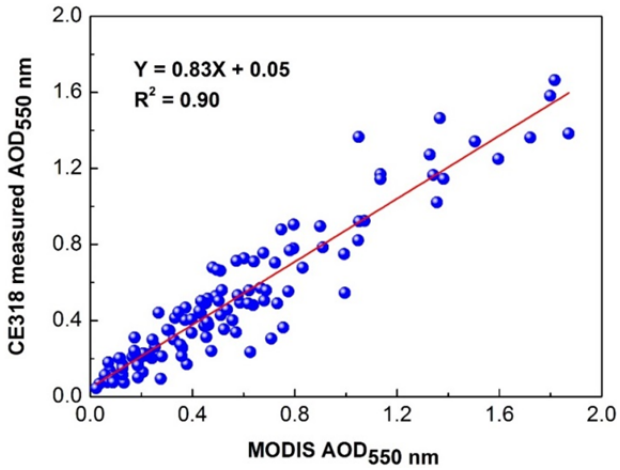

Fig. 2. Linear relationships between sunphotometer measured AOD_{550nm} and MODIS retrieval at Mount Song.

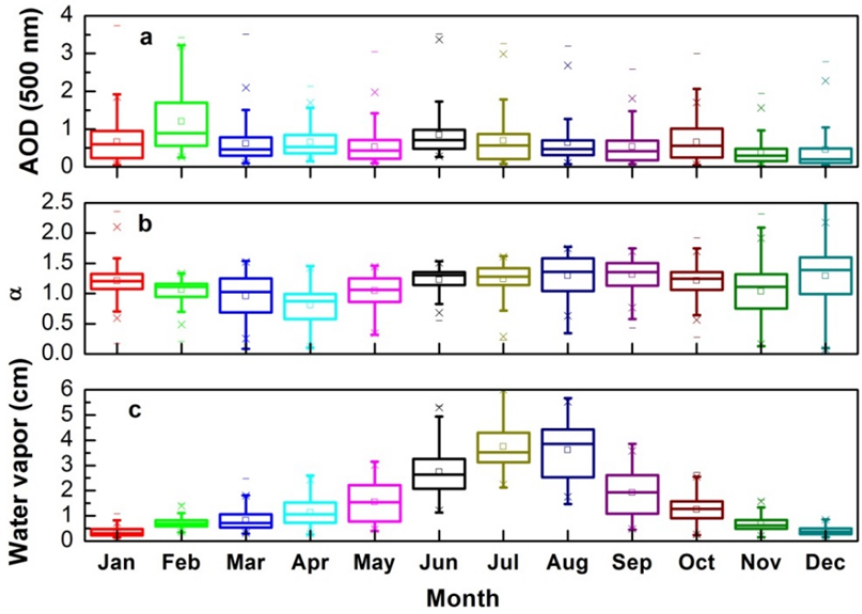

Fig. 3. Monthly variations of AOD and Ångström exponent at Mount Song.

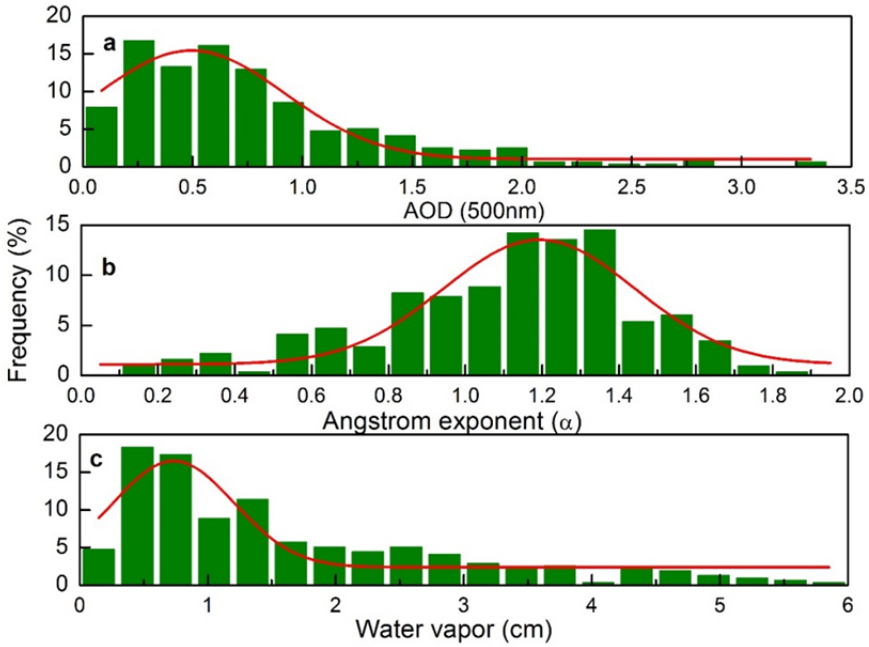

Fig. 4. Frequency distribution of $AOD_{500\ nm}$, Ångström exponent and water vapor at Mount Song.

similar results are also observed in Dunhuang and Lanzhou cities in China (Xia *et al.*, 2004; Yu *et al.*, 2009b).

Fig. 4 shows the frequency distribution of $AOD_{500\ nm}$ at the Mount Song during April 2012 to May 2014, AOD probability distribution is rather narrow with a modal value of 0.5, approximately 40% of the AOD is less than 0.5; the highest frequency value is 16% for AOD around 0.6; the accumulated frequency distribution is 72% with the AODs values in the range 0.20–1.0. This AOD distribution can be compared with other sites in China, for example, 82% of AOD varies in the range 0.17–0.45 at Dunhuang (Zheng *et al.*, 2008); nearly 60% of AOD varies in the range 0.2–0.5 at Yulin (Che *et al.*, 2009); the accumulated AOD frequency in the range 0.20–0.50 is about 65% at Longfengshan station (Wang *et al.*, 2010).

The probability maximum distribution of α (Fig. 4(b)) is around 1.35 with 15% frequency, approximately 90% of α varies in the range 0.6–1.6. Values of α greater than 1.6 and α values less than 0.8 accounted respectively for 1.3% and 8.2% of the total. It is reported that the probability distribution of α has a modal value of 1.1 and varies in the range 0 to 1.7 over Loess Plateau of Northwestern China (Bi *et al.*, 2011); values of α greater than 1.8 and less than 0.6 accounted respectively, for 0.3% and 1%, over Shanghai,

China (He *et al.*, 2012). Meanwhile, the frequency histogram of WVC shows a maximum around 0.6 cm; 75% lower than 2 cm and 64% in the range 0.3–1.8 cm (Fig. 4(c)).

Fig. 5(a) and Table 2 show the frequency distributions of $AOD_{500\ nm}$ for the four seasons at Mount Song, about 35%, 28%, 45% and 37% of the AODs values in the range 0.0–0.5 respectively, during spring, summer, autumn and winter seasons. During the spring season, more than 96% of AOD is higher than 0.18, and nearly 76% of AOD is lower than 1.0. The AOD distribution during summer is wider with one modal value of 0.7, varying between 0 and 3.3, and approximately 69% of AOD is lower than 1.0. The distribution of AOD is unimodal centered at 0.25 during autumn, 12% of AOD is lower than 0.18 and 19% values are higher than 1.0. Two AODs peaks are seen in the frequency distribution during winter season are likely due to the complexity of the aerosol sources during this season, 37% of the values are less than 0.5, and 66% values are less than 1.0. Similar analysis at other locations in China at Loess Plateau (Zheng *et al.*, 2008; He *et al.*, 2012) shows AODs variations in the range 0.2–1.7 and 0.2–1.5, respectively during spring and winter seasons are less than the values observed at the Mount Song (Bi *et al.*, 2011),.

Fig. 5(c) and Table 3 show the frequency distributions of α for all the four seasons at Mount Song, during spring, the distribution varies in the range 0.9–1.3 with two maxima peaks around 1, 32% of the α values are less than 0.8 and 68% in the range 0.8–1.6. The summer season shows small probability distribution of α with the modal value of 1.36; nearly 91% of α values vary in the range 0.8–1.6 and 60% in the range 1.0–1.4. The α values less than 1 for 15% and 12%, respectively are observed during autumn and winter seasons; 73% during autumn is in the range 1.0–1.7, and 82% during winter season in the range 0.8–1.6. Meanwhile, the column-integrated water vapor contents show significant seasonal variations (Fig. 5(b)). Only 8% of WVC is higher than 2.4 cm and 83% of the values vary in the range 0.3–2.0 cm during spring (Table 4). The frequency distribution of WVC during summer is in the range 1.3–5.9 cm, 95% of the WVC is higher than 2.0 cm and 48% are even higher than 3.6 cm during summer season when rainfall is more frequently occur. Similarly 84% of the WVC values are in the range 0.2–2.4 cm and only 5% of WVC is higher than 3.0 cm during autumn. The distribution of WVC is very small during winter season, 94% of the values are less than 1.0 cm, and 66% varies in the range 0.3–0.8 cm.

Single Scattering Albedo

The single scattering albedo (SSA) is a common measurement of the relative contribution of scattering to extinction, which is mostly dependent on the chemical composition, matter concentration and size distribution of

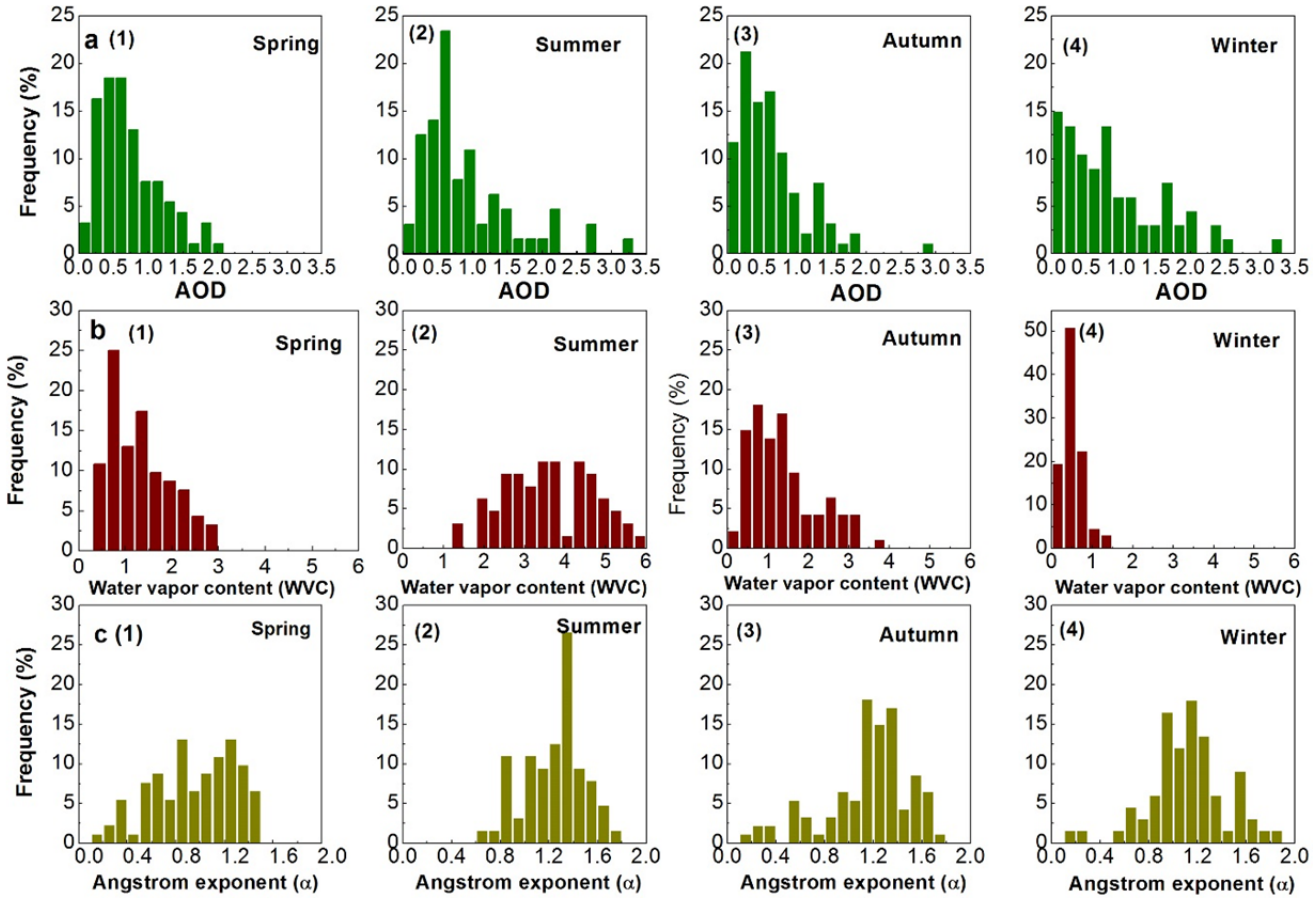

Fig. 5. Frequency distribution of $AOD_{500\ nm}$ (a), water vapor (b) and Ångström exponent (c) in different seasons at Mount Song.

Table 2. Frequency statistics of AOD values at each season at Mount Song (%).

	0–0.5	0.5–1	1–1.5	1.5–2	2–
Spring	35	41	18	4	1
Summer	28	40	16	6	9
Autumn	45	36	13	5	1
Winter	37	28	12	15	7

Table 3. Frequency statistics of Ångström exponent at each season at Mount Song (%)

	0–0.4	0.4–0.8	0.8–1.2	1.2–1.6	1.6–2.0
Spring	9	23	39	29	
Summer		3	34	56	6
Autumn	5	10	33	45	7
Winter	3	9	52	30	6

Table 4. Frequency statistics of water vapor at each season at Mount Song (%)

	0–1.2	12–2.4	2.4–3.6	3.6–4.8	4.8–6.0
Spring	49	43	8		
Summer		14	38	33	16
Autumn	49	35	15	1	
Winter	97	3			

aerosol particles (Dubovik *et al.*, 2002; Liu *et al.*, 2011). Fig. 6(a) shows the statistics of SSAT, SSAF and SSAC (single scattering albedo for total, fine and coarse particles) at the Mount Song, the mean SSAT at 440, 670, 870 and 1020 wavelengths, respectively are 0.90 ± 0.06, 0.91 ± 0.06, 0.90 ± 0.06 and 0.90 ± 0.07; the mean values of SSAF, respectively are 0.93 ± 0.04, 0.94 ± 0.04, 0.93 ± 0.06 and 0.92 ± 0.07; and the mean SSAC respectively, are 0.76 ± 0.1, 0.84 ± 0.08, 0.86 ± 0.08 and 0.88 ± 0.08. The SSAC is less than SSAT and SSAF, which indicates decrease in the scattering contribution of coarse particles. The average value for SSA is not dependent on the wavelength but the range of this change shows difference at different wavelengths, such characteristics are also observed in the Northern parts of China by Xia *et al.* (2005). The observed values of SSA are also compared with the SSA values observed at Xianghe, Beijing, Taihu, Xinglong, Guangzhou, Shanghai and Lanzhou in China, the difference in SSA values are likely due to the biomass burning, type of aerosol formation, long-distance transport and the meteorological conditions (Li *et al.*, 2007; Xia *et al.*, 2007; Cheng *et al.*, 2008; Bi *et al.*, 2011; He *et al.*, 2012; Zhu *et al.*, 2014).

Fig. 6(b) shows the monthly variations of SSAT, SSAF and SSAC at the wavelength 440 nm, the highest monthly mean SSAT is 0.94 in the month of February. The mean SSAT is 0.89 ± 0.04, 0.91 ± 0.06, 0.89 ± 0.07 and 0.92 ± 0.05 respectively, during spring, summer, autumn and winter seasons. Use of fossil fuel for heating purpose causes high scattering due to sulphate emissions show high SSAT. Due to biomass burning during October and November, low SSA (SSAF) values are observed mainly due to black carbon and organic substances (Singh, 2010). The aerosol hygroscopic growth due to relatively high atmospheric humidity also leads to higher SSAT during summer season (Gautam *et al.*, 2007; Zhao *et al.*, 2013; Wang *et al.*, 2015). The mean SSAF is 0.93 ± 0.03, 0.93 ± 0.03, 0.92 ± 0.05 and 0.94 ± 0.05, respectively are observed during spring, summer, autumn and winter seasons, which indicate more scattering of the fine-mode particles during winter season due to the hygroscopic sulfates and nitrates produced from the anthropogenic emissions (Wang *et al.*, 2011; Xin *et al.*, 2014). The monthly mean SSAC is less than 0.80, the highest monthly mean value 0.80 ± 0.08 in the month of February and the lowest monthly SSAC 0.73 ± 0.06 in the month of October. The seasonal mean SSAC is 0.76 ± 0.07, 0.75 ± 0.07, 0.74 ± 0.09 and 0.78 ± 0.1 respectively during spring, summer, autumn and winter. The mean SSAC during spring and winter is higher compared to those in other seasons, which is likely to be associated with the dominance of coarse particles associated with dust events when coarse particles are transported from surrounding Asian continent by the strong winds (Ge *et al.*, 2010, Cao *et al.*, 2014).

The frequency distributions of SSAT, SSAF and SSAC (440 nm) at Mount Song (Fig. 6(c)) show a single peak frequency distribution for SSAT with the peak value around 0.89, accounting 19% of the total occurrence. 86% of SSAT is higher than 0.85, the most frequent distribution in the range 0.89–0.96 is accounting for 62% of total occurrences, which indicate presence of strong aerosol scattering particles in this area. Similarly, 95% of the SSAF is higher than 0.89, the peak value is around 0.95, accounting for 25% of the total occurrences, the most frequent distribution of SSAF is in the range 0.91–0.99, accounting for 91% of the total occurrences. The frequency distribution of SSAC differ from those of SSAT and SSAF, the most frequent distribution of SSAC in the range 0.72–0.77, accounting 28% of the occurrences; 65% of SSAC is less than 0.8, indicates strong absorption from the presence of coarse-mode particles.

The relationship between AOD and SSA for total, fine and coarse particles (440 nm) (Fig. 7) at Mount Song show

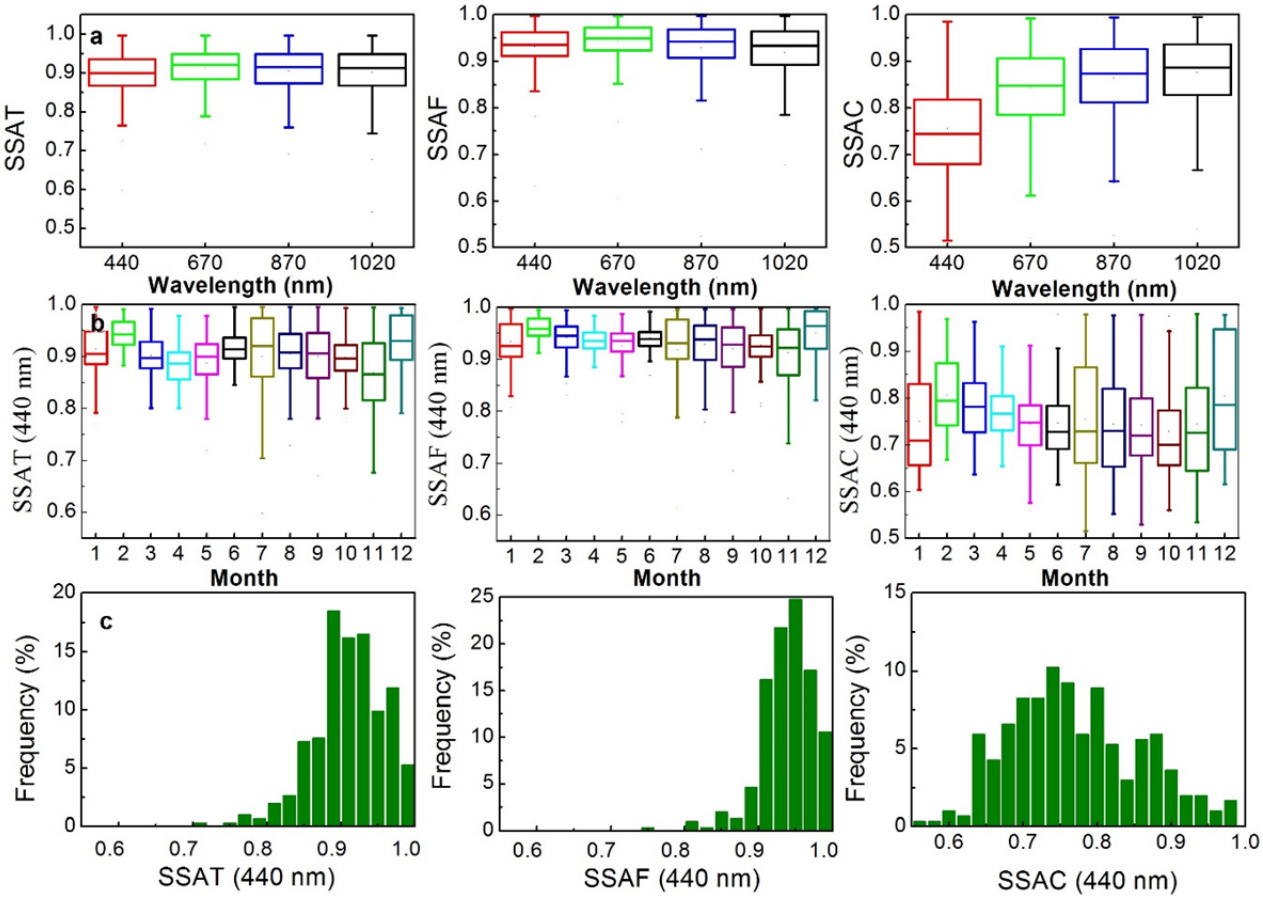

Fig. 6. (a) Distributions of SSAT, SSAF and SSAC at Mount Song; (b) Monthly variations of SSAT, SSAF and SSAC at Mount Song; (c) Frequency distributions of SSAT, SSAF and SSAC at Mount Song.

the distributions of SSAT, SSAF and SSAC in different ranges of AOD, the average SSAT generally increases with AOD, the lowest (average) SSAT is 0.88 ± 0.04 when AOD varies in the range 0.3–0.6, the largest (average) SSAT value 0.97 ± 0.01 when AOD varies in the range of 2.7–3.0. This observation shows that the mean SSAT is generally larger than 0.90 and the scattering capacity increases with AOD at this rural site in Central China. Similarly, the mean SSAF varies in the range 0.93–0.98, the low and high SSAF is observed respectively, for AOD in the range 0.3–0.6 and 2.7–3.0. The hygroscopic growth of aerosols increase the radius of the fine-mode particles that enhances the value of SSA with higher AOD. Generally, SSAC is much smaller compared to SSAT and SSAF for each range of AOD and the high value of SSAC (0.89 ± 0.02); SSAC is lower than 0.8 corresponds to the AOD value less than 1.8 shows higher absorption due to the presence of coarse particles.

Fig. 8 shows relationship between AOD, SSA and α, when AOD is less than 0.5, SSAT for most of the particles with $\alpha > 1.0$ higher than 0.9, while SSAT for larger particles with $\alpha \leq 1.0$ is less than 0.9. This indicates high absorption for coarse particles with high scattering for fine-mode particles. When AOD varies 0.5–1.0, 1.0–1.5, and 1.5–2.0, the SSAT is higher than 0.9, shows increasing scattering for both fine and coarse particles. Higher AODs show high atmospheric pollution could be due to dominance of fine particles associated with anthropogenic activities in this region.

Aerosol Size Distribution

The aerosol size distribution differs with the season due to the combustion state, fuel properties, burning material and intensity, environmental temperature and relative humidity. The aerosol volume size distributions are generally bimodal with strong seasonal variability, which represents aerosol mixing. The fine mode shows the maxima peak of radius 0.14–0.15 μm during spring and autumn, and radius range 0.19–0.25 μm during summer and winter seasons (Fig. 9(a)). The coarse mode shows a distinct difference in the radius of aerosol particles, the maxima peak of radius 1.7–2.2 μm during spring, 2.9–3.8 μm during summer, and 2.2–2.9 μm during autumn and winter seasons. Fig. 9 clearly shows dominance of the coarse mode particles (radius 2.2–3.8 μm) during spring (and winter) this could be associated with the transport of air mass from the dust events (Fig. 9(c)) and fine-mode particles (0.19–0.25 μm) during summer due to the growth of hygroscopic particle when the relative humidity is highest. As shown in Fig. 9(a), the coarse aerosol particles dominance during spring season, the back trajectories computed from NOAA HYSPILT (http://ready.arl.noaa.gov/HYSPLIT.php) clearly show air mass from desert areas (Fig. 9(c)) reaching at the Mount Song during spring season.

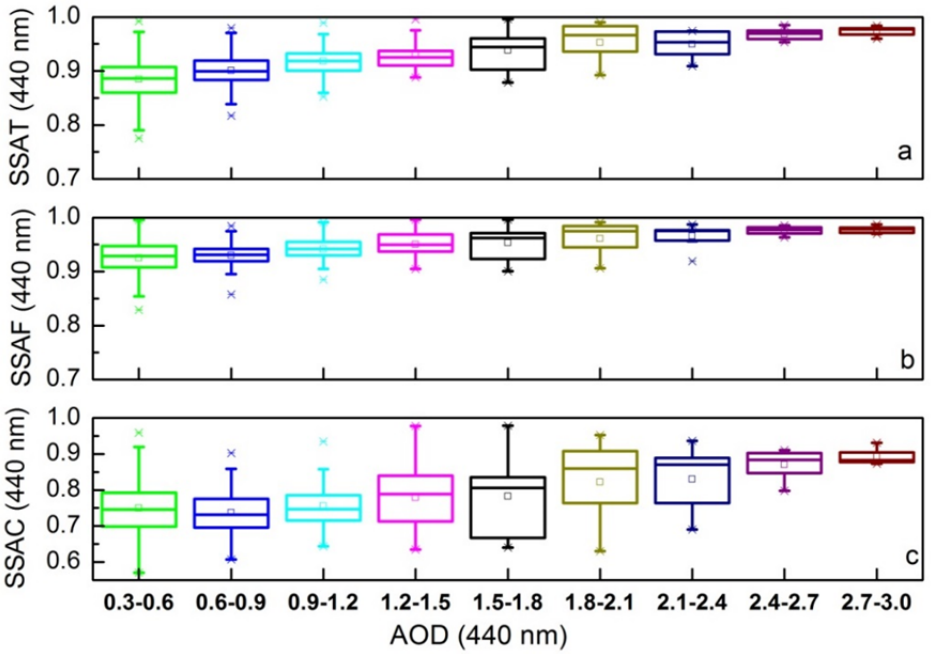

Fig. 7. Relationship between AOD and SSA (SSAT, SSAF and SSAC).

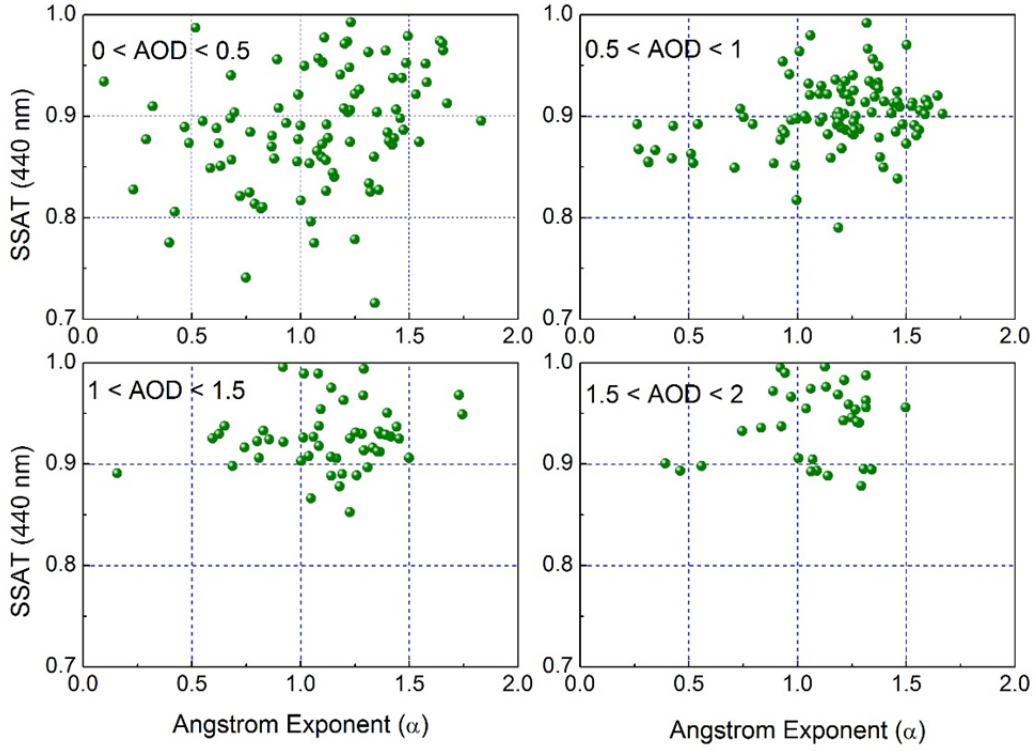

Fig. 8. Relationship between AOD, SSA and Ångström exponent.

The size distribution of particles show bimodal pattern (dominance of aerosol size in fine and coarse modes), an increase in fine-mode volume concentration is observed with increasing AOD, e.g., the maxima peak at radius 0.11, 0.15, 0.15, 0.15, 0.26 and 0.26 μm, respectively, for AOD range 0–0.2, 0.2–0.4, 0.4–0.6, 0.6–0.8, 0.8–1.0 and > 1.0 (Fig. 9(b)).

Aerosol Refractive Index

The real part of refractive index represents scattering capacity and the imaginary part represents the absorption capacity that is closely related to hygroscopic properties, humidity and the aerosol chemical compositions (Dubovik and King, 2000, Singh *et al.*, 2004). The real and imaginary parts of the refractive index retrieved for the wavelengths

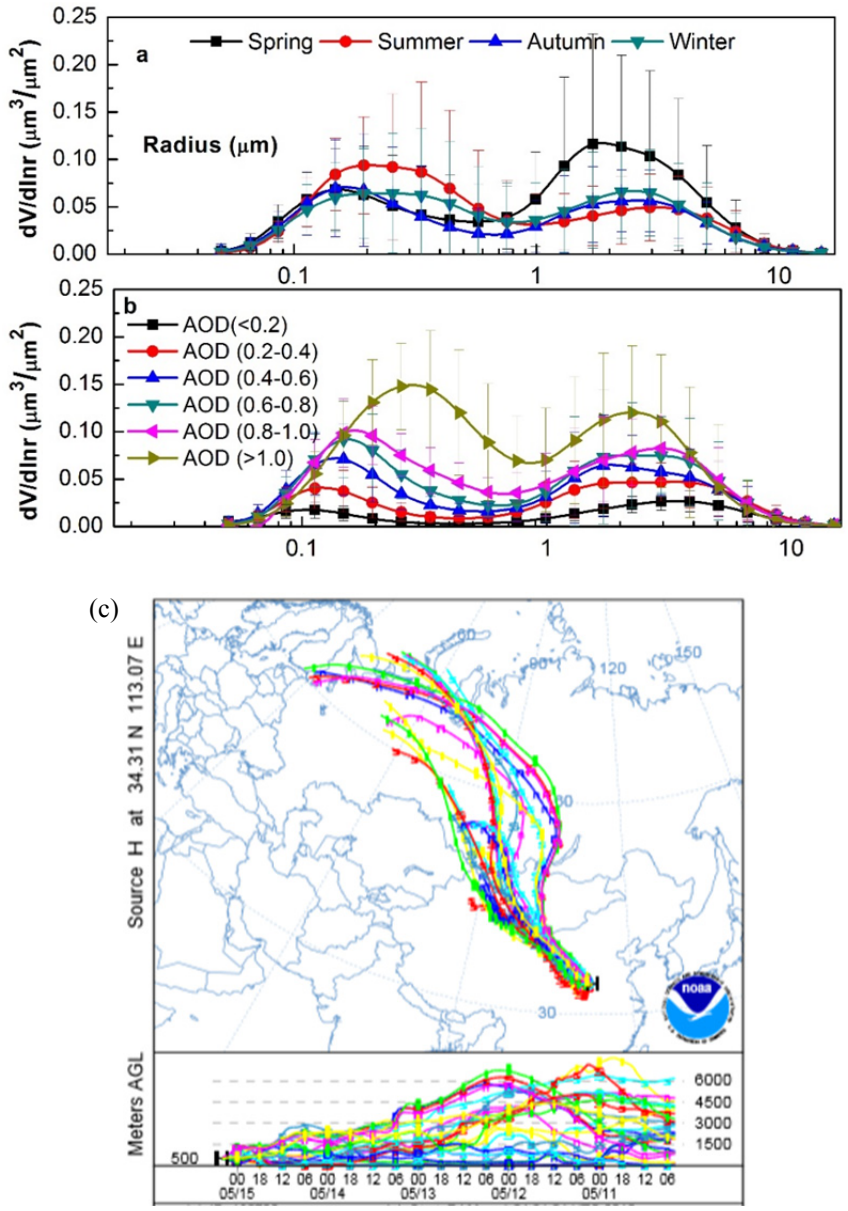

Fig. 9. (a) Seasonal variations of aerosol size distributions; (b) Relationship between aerosol size distribution and AOD; (c) Back trajectories showing air mass at the Mount Song during spring season from Desert region.

(440, 675, 870 and 1020 nm) correspond to sky radiance measurements are considered respectively in the range 1.33–1.60 and 0.0005–0.50 (Dubovik *et al.*, 2000; Che *et al.*, 2008, 2009). Fig. 10 shows seasonally averaged refractive index (real and imaginary parts) at wavelengths 440, 675, 870 and 1020 nm during the period 2012–2014 over rural Central China. The real part of refractive index (Fig. 10(a)) increases with wavelengths, such behavior show highly scattering nature of aerosols due to the presence of coarse particles in the near infrared in a given AODs values (Cheng *et al.*, 2006). The real part of the refractive index is smaller during summer season compared to other seasons, and in all seasons the real part shows a strong wavelength dependence, for example, the real part of the refractive index increases drastically from 1.421 at the wavelength 440 nm to 1.458 and wavelength 1020 nm during summer. The real part values are generally higher during spring season (1.476, 1.493, 1.507 and 1.510, respectively at wavelengths 440, 675, 870 and 1020 nm).

The imaginary part of refractive index (Fig. 10(b)) shows highest values at the wavelength 400 nm and afterwards decreases drastically at wavelength 675 nm. In the wavelength range 870–1020 nm, a slightly increase in the imaginary part is observed in the wavelength range 870–1020 nm during all seasons except spring season shows almost constant value showing no wavelength dependency. The imaginary part of refractive index at the Mount Song are found to be higher during autumn and winter seasons compared to those of spring and summer seasons. The decrease in the imaginary part of refractive index is likely related to the hygroscopic growth in the summer season and due to the presence of dust during spring season.

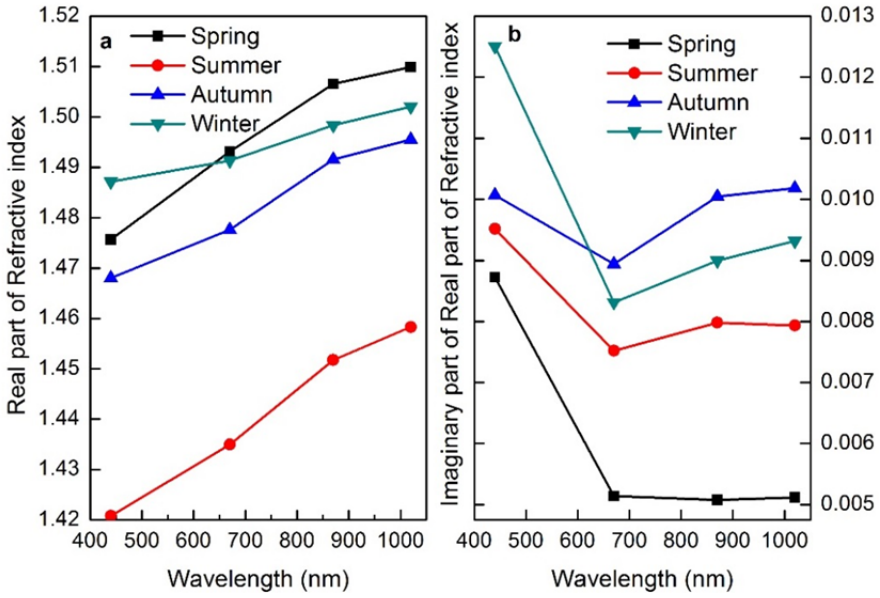

Fig. 10. Seasonal variations of (a) real part and (b) imaginary part of refractive index.

CONCLUSIONS

The aerosol optical and microphysical properties are measured first time at the Mount Song, a rural site in Central China. Detailed analysis of sun photometer data are analyzed for the two years period. The monthly and seasonal variations of AODs, Ångström exponent, water vapor, single scattering albedo (for total, fine and coarse particles), aerosol size distribution and refractive index (real part and imaginary parts) show characteristics variations.

The monthly average AOD_{500nm} increases from autumn and winter to summer seasons, the seasonal mean AOD_{500nm} values are 0.6 ± 0.42, 0.72 ± 0.52, 0.51 ± 0.42 and 0.64 ± 0.58, respectively, for spring, summer, autumn and winter seasons; the average value of AOD is highest during summer season. The monthly average of α is generally larger than 0.8, the smallest value (0.81 ± 0.30) of α in the month of April and the highest 1.32 ± 0.23 in the month of September due to the difference sources of air mass reaching at mount Song. The monthly mean WVC increases from 0.35 cm in the month of January to 3.62 cm in the month of August with annual average value about 1.625 cm at this rural site in Central China. The single peak distribution for AOD, α and WVC are 40% of the AOD is smaller than 1 and 72% of the AOD in the range 0.2–1.0; 90% of α in the range 0.6–1.6 and the maxima peak value of 1.35 at Mount Song.

The monthly mean SSA is generally higher during winter and summer seasons, SSAT values are 0.89 ± 0.04, 0.91 ± 0.06, 0.89 ± 0.07 and 0.92 ± 0.05 respectively, during spring, summer, autumn and winter seasons. The seasonal characteristics may relate to local biomass burning, anthropogenic emissions transported from outside and the aerosol hygroscopic properties. SSAF was similar for all the seasons, 95% of the SSAF is higher than 0.89 and the most frequent distribution was in the range 0.91 and 0.99, accounting for 91% of the total occurrences. The relationship between AOD, SSA and α at Mount Song further indicates that the aerosol scattering capacity increases with AOD, for example, the SSAT is generally larger than 0.9 when AOD is higher than 0.5.

The aerosol volume size distributions are generally bimodal normal structures with significant seasonal variability in volume concentration and peak radius. The fine-mode particles show the maxima peak at radius 0.14–0.15 μm during spring and autumn, and radius 0.19–0.25 μm during summer and winter seasons. The size distribution shows a distinct difference in dominant mode for different seasons, for example, the coarse-mode particles are dominant during spring which could be associated with the presence of dust particles. Meanwhile, it is observed that the real part of refractive index increases with wavelengths in each season and the average of real part is slightly higher during spring and winter seasons. The imaginary part of refractive index decreases from wavelength 400 nm to 675 nm and afterwards slightly increases in the wavelength range 870–1020 nm for all seasons except in summer season when imaginary part is almost constant.

The present results show the monthly and seasonal characteristic of columnar aerosol optical properties at the Mount Song, which is very important to evaluate the aerosol climate effects. The results presented in the present paper is the first result at this site which is a rural site in Central China, the aerosol compositions and direct and indirect radiative effects will be investigated in future studies by combining long-term aerosol observations and radiative transfer simulations.

ACKNOWLEDGMENTS

The present study is supported through research grant No. 2011CB707106 sponsored by National Basic Research Program (research grants No. 41127901) and National Natural Science Foundation of China (NSFC) (No. 41401631) and through the Special Fund for Basic Scientific Research

of Central Colleges, China University of Geosciences, Wuhan. We thank all members of Lidar team in Liesmars, Wuhan University, China. We are grateful to anonymous referees and the editor Dr. James Campbell and Dr. Lin-Chi Wang for their valuable comments/suggestions which helped us to improve the earlier version of the manuscript. The authors are also grateful to NASA GIOVANNI team for providing data through their website and NOAA HYSPLIT for back trajectories to see the tracks of air mass.

REFERENCES

Albrecht, B. (1989). Aerosols, Cloud Microphysics, and Fractional Cloudiness. *Science* 245: 1227–1230.

Bi, J., Huang, J.P., Qiang, F., Wang, X., Shi, J., Zhang, W., Huang, Z. and Zhang, B. (2010). Toward Characterization of the Aerosol Optical Properties over Loess Plateau of Northwestern China. *J. Quant. Spectrosc. Radiat. Transfer* 112: 346–360.

Breon, F., Tanré, D. and Generoso, S. (2002). Aerosols Effect on the Cloud Droplet Size Monitored from Satellite. *Science* 295: 834–838.

Cao, C., Zheng, S. and Singh, R.P. (2014). Characteristics of Aerosol Optical Properties and Meteorological Parameters during Three Major Dust Events (2005–2010) over Beijing, China. *Atmos. Res.* 150: 129–142.

Che, H., Wang, Y., Sun, J., Zhang, X., Zhang, X. and Guo, J. (2013). Variation of Aerosol Optical Properties over the Taklimakan Desert in China. *Aerosol Air Qual. Res.* 13: 777–785.

Che, H., Zhang, X., Chen, H., Damiri, B., Goloub, P., Li, Z., Zhang, X., Wei, Y., Zhou, H., Dong, F., Li, D. and Zhou, T. (2009). Instrument Calibration and Aerosol Optical Depth (AOD) Validation of the China Aerosol Remote Sensing Network (CARSNET). *J. Geophys. Res.* 114, doi: 10.1029/2008JD011030.

Che, H., Zhang, X.Y., Xia, X., Goloub, P., Holben, B., Zhao, H., Wang, Y., Zhang, X.C., Wang, H., Blarel, L., Damiri, B., Zhang, R., Deng, X., Ma, Y., Wang, T., Geng, F., Qi, B., Zhu, J., Yu, J., Chen, Q. and Shi, G. (2015). Ground-Based Aerosol Climatology of China: Aerosol Optical Depths from the China Aerosol Remote Sensing Network (CARSNET) 2002–2013. *Atmos. Chem. Phys.* 15: 7619–7652.

Che, H.Z., Shi, G., Uchiyama, A., Yamazaki, A., Chen, H., Goloub, P. and Zhang, X. (2008). Intercomparison between Aerosol Optical Properties by a PREDE Skyradiometer and CIMEL Sunphotometer over Beijing, China. *Atmos. Chem. Phys.* 8: 3199–3214.

Che, H., Xia, X., Zhu, J., Li, Z., Dubovik, O., Holben, B., Goloub, P., Chen, H., Estelles, V., Cuevas-Agulló, E., Blarel, L., Wang, H., Zhao, H., Zhang, X., Wang, Y., Sun, J., Tao, R., Zhang, X. and Shi, G. (2014a). Column Aerosol Optical Properties and Aerosol Radiative Forcing during a Serious Haze-fog Month over North China Plain in 2013 Based on Ground-based Sunphotometer Measurements, *Atmos. Chem. Phys.* 14: 2125–2138, doi: 10.5194/acp-14-2125-2014.

Che, H., Xia, X., Zhu, J., Wang, H., Wang, Y.Q., Sun, J.Y., Zhang, X.C., Zhang, X.Y. and Shi, G.Y. (2014b). Aerosol Optical Properties under the Condition of Heavy Haze over an Urban Site of Beijing, China. *Environ. Sci. Pollut. Res*. 22: 1043–1053, doi: 10.1007/s11356-014-3415-5.

Chen, J., Jiang, H., Wang, B., Xiao, Z.Y., Jiang, Z.S., Zhou, G.M. and Yu, S.Q. (2012). Aerosol Optical Properties from Sun Photometric Measurements in Hangzhou District, China. *Int. J. Remote Sens.* 33: 2451–2461.

Cheng, T.T., Liu, Y., Lu, D.R., Xu, Y.F. and Li, H.Y. (2006). Aerosol Properties and Radiative Forcing in Hunshan Dake Desert, Northern China. *Atmos. Environ.* 40: 6351–6372.

Cheng, Y., Wiedensohle, A. and Eichler, H. (2008). Aerosol Optical Properties and Related Chemical Apportionment at Xinken in Pearl River Delta of China. *Atmos. Environ.* 42: 2169–2179.

Dubovik, O., Holben, B., Eck, T.F., Smirnov1, A., Kaufman, Y.J., King, M.D. and Slutsker, I. (2002). Variability of Absorption and Optical Properties of Key Aerosol Types Observed in Worldwide Locations. *J. Atmos. Sci.* 59: 590–608.

Dubovik, O. and King, M.D. (2000). A Flexible Inversion Algorithm for Retrieval of Aerosol Optical Properties from Sun and Sky Radiance Measurements. *J. Geophys. Res*. 105: 20673–20696.

Dubovik, O., Sinyuk, A., Lapyonok, T., Holben, B.N., Mishchenko, M., Yang, P., Eck, T.F., Volten, H., Muñoz, O., Veihelmann, B., van der Zande, W.J., Leon, J.F., Sorokin, M. and Slutsker, I. (2006). Application of Spheroid Models to Account for Aerosol Particle Nonsphericity in Remote Sensing of Desert Dust. *J. Geophys. Res*. 111, doi: 10.1029/2005jd006619.

Dubovik, O., Smirnov, A., Holben, B.N., King, M.D., Kaufman, Y.J., Eck, T.F. and Slutsker, I. (2000). Accuracy Assessments of Aerosol Optical Properties Retrieved from Aerosol Robotic Network (AERONET) Sun and Sky Radiance Measurements. *J. Geophys. Res*. 105: 9791–9806.

Eck, T.F., Holben, B.N., Dubovik, O., Smirnov, A., Goloub, P., Chen, H.B., Chatenet, B., Gomes, L., Zhang, X.Y., Tsay, S.C., Ji, Q., Giles, D. and Slutsker, I. (2005). Columnar Aerosol Optical Properties at AERONET Sites in Central Eastern Asia and Aerosol Transport to the Tropical Mid-Pacific, *J. Geophys. Res.* 110: D06202, doi: 10.1029/2004JD005274.

Eck, T.F., Holben, B.N., Reid, J.S., Dubovik, O., Smirnov, A., O'Neill, N.T., Slutsker, I. and Kinne, S. (1999). Wavelength Dependence of the Optical Depth of Biomass Burning, Urban, and Desert Dust Aerosols. *J. Geophys. Res.* 104: 31333–31349.

Eck, T.F., Holben, B.N., Sinyuk, A., Pinker, R.T., Goloub, P., Chen, H., Chatenet, B., Li, Z., Singh, R.P., Tripathi, S.N., Reid, J.S., Giles, D.M., Dubovik, O., O'Neill, N.T., Smirnov, A., Wang, P. and Xia, X. (2010). Climatological Aspects of the Optical Properties of Fine/Coarse Mode Aerosol Mixtures. *J. Geophys. Res.* 115, doi: 10.1029/2010JD014002.

Estellés, V., Campanelli, M., Utrillas, M.P., Expósito, F. and Martinez-Lozano, J.A. (2012). Comparison of AERONET

and SKYRAD4.2 Inversion Products Retrieved from a Cimel CE318 Sunphotometer. *Atmos. Meas. Tech.* 5: 569–579.

Gautam, R., Hsu, N.C., Kafatos, M. and Tsay, S.C. (2007). Influences of Winter Haze on Fog/Low Cloud over the Indo-Gangetic Plains, *J. Geophys. Res.* 112: D05207.

Ge, J.M., Su, J., Ackerman, T.P., Fu, Q., Huang, J.P. and Shi, J.S. (2010). Dust Aerosol Optical Properties Retrieval and Radiative Forcing over Northwestern China during the 2008 China-U.S. Joint Field Experiment. *J. Geophys. Res.* 115: D00K12, doi: 10.1029/2009JD013263.

Goloub, P., Li, Z., Dubovik, O., Blarel, L., Podvin, T., Jankowiak, I., Lecoq, R., Deroo, C., Chatenet, B., Morel, J.P., Cuevas, E. and Ramos, R. (2007). PHOTONS/AERONET Sunphotometer Network Overview: Description, Activities, Results. *Proc. SPIE* 6936: 69360V, doi: 10.1117/12.783171.

Guo, J.P., Zhang, X.Y., Wu, Y.R., Zhaxi, Y.Z., Che, H.Z., La, B., Wang, W. and Li, X.W. (2010). Spatio-temporal Variation Trends of Satellite-based Aerosol Optical Depth in China during 1980-2008. *Atmos. Environ.* 45: 6802–6811.

He, Q., Li, C., Geng, F., Yang, H., Li, P., Li, T., Liu, D. and Pei, Z. (2012). Aerosol Optical Properties Retrieved from Sun Photometer Measurements over Shanghai, China. *J. Geophys. Res.* 117: D16204, doi: 10.1029/2011JD017220.

Holben, B.N., Eck, T.F., Slutsker, I., Tanre, D., Buis, J.P., Setzer, A., Vermote, E., Reagan, J.A., Kaufman, Y.J., Nakajima, T., Lavenu, F., Jnnkowiak, I. and Smirnov, A. (1998). AERONET-A Federated Instrument Network and Data Archive for Aerosol Characterization. *Remote Sens. Environ.* 66: 1–16.

IPCC (2007). Summary for Policymakers. Climate Change 2007: The Physical Science Basis. Contribution of Working Group I to the Fourth Assessment Report of the Intergovernmental Panel on Climate Change, Solomon, S., Qin, D., Manning, M., Chen, Z., Marquis, M., Averyt, K.B., Tignor, M. and Miller, H.L. (Eds.), Cambridge University Press: Cambridge, United Kingdom and New York, USA.

Kumar, S., Singh, A.K., Prasad, A.K. and Singh, R.P. (2013). Variability of GPS Derived Water Vapor and Comparison with MODIS Data over the Indo-Gangetic Plains. *Phys. Chem. Earth.* 55–57: 11–18.

Lao, Z.Q. and Wang, S.Y. (1999). New Advances in the Study of the Dengfeng Complex in the Songshan Region, Henan Province. *Reg. Geol. China* 18: 9–16.

Li, H.F., Zhao, H.Q., Zhou, X.F., Li, X.H. and Li, S.Z. (2008). Characteristic Analysis of the Rainstorm over Dengfeng in Spring 2007. *Meteorol. Environ. Sci.* 31: 61–65.

Li, Z., Xia, X.A., Cribb, M., Mi, W., Holben, B., Wang, P.C., Chen, H.B., Zhao, F.S. and Dickerson, R.E. (2007). Aerosol Optical Properties and Their Radiative Effects in Northern China. *J. Geophys. Res.* 112: D22S01, doi: 10.1029/2006JD007382.

Li, Z.Z., Xu, W., Fu, Q.Y., Min, X.J., Zhang, L.M., Pan, Z.Q., Qiao, Y.L., Zheng, X.B., Fan, Y.T., Su, B.J. and Han, Q.J. (2014). Building and Application for China Songshan Artificial Target Site. *J. Atmos. Environ. Opt.* 9: 81–89.

Liu, Y., Huang, J.P., Shi, G.Y., Takamura, T., Khatri, T., Bi, J., Shi, J., Wang, T. and Zhang, B. (2011). Aerosol Optical Properties and Radiative Effect Determined from Sky-radiometer over Loess Plateau of Northwest China. *Atmos. Chem. Phys.* 11: 11455–11463.

Liu, Z.W., Chen, L.L., Kang, Y.B., Ling, B.X. and Sun, K.Q. (2012). Study on Resource Management and Sustainable Development of World Cultural Heritage in China. A Case of Historic Monuments of Dengfeng in the Centre of Heaven and Earth. *Resour. Dev. Market* 28: 59–62.

Lu, S., Liu, Y., Long, H. and Guan, X. (2013). Agricultural Production Structure Optimization: A Case Study of Major Grain Producing Areas, China. *J. Integr. Agr.* 12: 184–197.

Pan, L., Che, H.Z., Geng, F.H., Xia, X.G., Wang, Y.Q., Zhu, C.Z., Chen, M., Gao, W. and Guo, J.P. (2010). Aerosol Optical Properties Based on Ground Measurements over the Chinese Yangtze Delta Region. *Atmos. Environ.* 44: 2587–2596.

Prasad, A.K, and Singh, R.P. (20005). Comparison of MISR - MODIS Aerosol Optical Depth over the Indo-Gangetic Basin during the Winter and Summer Seasons (2000 - 2005). *Remote Sens. Environ.* 107:109–119.

Prasad, A.K. and Singh, R.P. (2009). Validation of MODIS Terra, AIRS, NCEP/DOE AMIP-II Reanalysis-2, and AERONET Sun Photometer Derived Integrated Precipitable Water Vapor Using Ground-based GPS Receivers over India. *J. Geophys. Res.* 114, doi: 10.1029/2008JD011230.

Singh, R.P. (2010). Interactive Comment on "Inferring Absorbing Organic Carbon Content from AERONET Data" by A. Arola *et al.*. *Atmos. Chem. Phys. Discuss.* 10: C7718–C7718.

Singh, R.P., Dey, S., Tripathi, S.N., Tare, V. and Holben, B.N. (2004). Variability of Aerosol Parameters over Kanpur, Northern India. *J. Geophys. Res.* 109, doi: 10.1029/2004JD004966.

Smirnov, A., Holben, B.N., Eck, T.F. and Dubovik, O., Slutsker, I. (2000). Cloud Screening and Quality Control Algorithms for the AERONET Database. *Remote Sens. Environ.* 73: 337–349.

Tao, R., Che, H.Z., Chen, Q.L., Tao, J., Wang, Y.Q., Sun, J.Y., Wang, H. and Zhang, X.Y. (2014a). Study of Aerosol Optical Properties Based on Ground Measurements over Sichuan Basin, China. *Aerosol Air Qual. Res.* 14: 905–915.

Tao, R., Che, H.Z., Chen, Q.L., Wang, Y.Q., Sun, J.Y., Zhang, X.C., Lu, S., Guo, J.P., Wang, H. and Zhang, X.Y. (2014b). Development of an Integrating Sphere Calibration Method for Cimel Sunphotometers in China Aerosol Remote Sensing Network. *Particuology* 13: 88–99.

Tripathi, S.N., Dey, S., Chandel, A., Srivastava, S., Singh, R.P. and Holben, B.N. (2005). Comparison of MODIS and AERONET Derived Aerosol Optical Depth over the Ganga Basin, India. *Ann. Geophys*. 23: 1093–1101.

Wang, L.C., Gong, W., Li, J., Ma, Y.Y. and Hu, B. (2014a). Empirical Studies of Cloud Effects on Ultraviolet Radiation in Central China. *Int. J. Climatol.* 34: 2218–2228.

Wang, L.C., Gong, W., Lin, A.W. and Hu, B. (2014b). Measurements and Cloudiness Influence on UV Radiation in Central China. *Int. J. Climatol.* 34: 3417–3425.

Wang, L.C., Gong, W., Xia, X.A., Zhu, J., Li, J. and Zhu, Z.M. (2015). Long-term Observations of Aerosol Optical Properties at Wuhan, an Urban Site in Central China. *Atmos. Environ.* 101: 94–102.

Wang, P., Che, H.Z., Zhang, X.C., Song, Q.I., Wang, Y.Q., Zhang, Z.H., Dai, X. and Yu, D.J. (2010). Aerosol Optical Properties of Regional Background Atmosphere in Northeast China. *Atmos. Environ.* 44*:* 4404–4412.

Wang, Y., Xin, J., Li, Z., Wang, S., Wang, P., Hao, W.H., Nordgren, B.L., Chen, H., Wang, L. and Sun, Y. (2011). Seasonal variations in Aerosol Optical Properties over China, *J. Geophys. Res.* 116: D18209, doi: 10.1029/2010JD015376.

Xia, X., Chen, H. and Wang, P. (2004). Aerosol Properties in a Chinese Semiarid Region. *Atmos. Environ.* 38: 4571–4581.

Xia, X.A., Chen, H.B., Wang, P.C., Zhang, W.X., Goloub, P., Chatenet, B., Eck, T.F. and Holben, B.N. (2006). Variation of Column-integrated Aerosol Properties in a Chinese Urban Region. *J. Geophys. Res.* 111: D05204, doi: 10.1029/2005JD006203.

Xia, X.A., Chen, H.B., Wang, P.C., Zong, X.M., Qiu, J.H. and Philippe, G. (2001). Aerosol Properties and Their Spatial and Temporal Variations over North China in Spring. *Tellus Ser. B* 57: 28–39

Xia, X.A., Li, Z., Holben, B., Wang, P., Eck, T., Chen, H., Cribb, M. and Zhao, Y. (2007). Aerosol Optical Properties and Radiative Effects in the Yangtze Delta Region of China, *J. Geophys. Res.* 112: D22S12, doi: 10.1029/2007JD008859.

Xin, J.Y., Zhang, Q., Gong, C.S., Wang, Y.S., Du, W.P. and Zhao, Y.F. (2014). Aerosol Direct Radiative Forcing over Shandong Peninsula in East Asia from 2004 to 2011. *Atmos. Oceanic Sci. Lett.* 7:74–79.

Yu, X.N., Zhu, B., Fan, S.X., Yin, Y. and Bu, X.L. (2009b). Ground-based Observation of Aerosol Optical Properties in Lanzhou, China. *J. Environ. Sci.* 21: 1519–1524.

Yu, X.N., Zhu, B. and Zhang, M.G. (2009a). Seasonal Variability of Aerosol Optical Properties over Beijing. *Atmos. Environ.* 43: 4095–4101.

Zhao, H.J., Che, H.Z., Zhang, X.Y., Ma, Y.J., Wang, Y.F., Wang, X.X., Liu, C., Hou, B. and Che, H.C. (2013). Aerosol Optical Properties over Urban and Industrial Region of Northeast China by Using Ground-based Sun-photometer Measurement. *Atmos. Environ.* 75: 270–278.

Zheng, S., Cao, C. X. and Singh, R. P. (2014). Comparison of Ground Based Indices (API and AQI) with Satellite Based Aerosol Products. *Sci. Total Environ.* 488: 398–412.

Zheng, Y.F., Liu, J.J., Wu, R.J., Li, Z.Q., Wang, B. and Tamio, T. (2008). Seasonal Statistical Characteristics of Aerosol Optical Properties at a Site near a Dust Region in China, *J. Geophys. Res.* 113: D16205, doi: 10.1029/2007JD009384.

Zhu, J., Che, H.Z., Xia, X.A., Chen, H.B., Goloub, P. and Zhang, W.X. (2014). Column-integrated Aerosol Optical and Physical Properties at a Regional Background Atmosphere in North China Plain. *Atmos. Environ.* 84: 54–64.

Zhuang, B.L., Wang, T.J., Li, S., Liu, J., Talbot, R., Mao, H.T., Yang, X.Q., Fu, C.B., Yin, C.Q., Zhu, J.L., Che, H.Z. and Zhang, X.Y. (2014). Optical Properties and Radiative Forcing of Urban Aerosols in Nanjing, China. *Atmos. Environ.* 83: 43–52.

Received for review, December 27, 2014
Revised, May 2, 2015
Accepted, August 11, 2015